Proceeding of the IEEE
International Conference on Robotics and Biomimetics
Dali, China, December 2019

# Industrial Robot Rotate Vector Reducer Fault Detection Based on Hidden Markov Models

Yinlong Zhang[1], Haibo An[2,*], Xiaojian Ding[3,] Wei Liang[2,*] *Senior Member, IEEE,* Mingze Yuan[1], Chunyang Ji[3] and Jindong Tan[4] *Member, IEEE*

***Abstract*— Reliable fault detection of rotate vector (RV) reducer is of paramount importance for the long-term maintenance of high-precision industrial robots. This paper proposes a Hidden Markov Model (HMM) based RV reducer fault detection using Acoustic Emission (AE) measurements. Compared with the conventional faults from the common rotating machinery (such as bearings and gears), the fault from the RV reducer is more complicated and undetectable due to its inherent inline and two-stage meshing structure. To this end, this work modifies the HMM model by taking into account not only the current observations and previous states, but also the subsequent series of observations within the posteriori probability framework. Through this way, the random and unknown disturbance, which is common in the industrial scenarios, could be reduced. Besides, the HMM is also applied to separate the AE signal bulks within one cycle that has 39 subcycles, which is a critical step for AE signal pre-processings. The proposed method has been evaluated on our collected AE signal dataset from the RV reducer in the industrial robotic platform. The experimental results and analysis validate that the proposed HMM based RV Reducer fault detection model can reliably and accurately detect reducer faults.**

## I. Introduction

Over the recent decades, fault detection has been playing an increasingly important role in the condition monitoring and timely maintenance of safety-critical robots, such as industrial robotic arms [1]–[3], manufacturing production lines [4]–[6]. The detection and intervention of industrial robots is now undertaken based on its health conditions rather than being checked regularly in a pre-set schedule. Through this way, the robotic core components could be continuously monitored and the operation efficiency could be improved.

1. Yinlong Zhang and Mingze Yuan are with Shenyang Institute of Automation, Guangzhou, Chinese Academy of Sciences, Guangzhou, 511548, China and with the Key Laboratory of Networked Control Systems, Shenyang Institute of Automation, Chinese Academy of Sciences, Shenyang, 110016, China and with Institutes for Robotics and Intelligent Manufacturing, Chinese Academy of Sciences, Shenyang 110016, China. email:{zhangyinlong, mzyuan}@sia.cn

2. Haibo An and Wei Liang (corresponding authors) are with the State Key Laboratory of Robotics, Shenyang Institute of Automation, Chinese Academy of Sciences, Shenyang 110016, China and with Key Laboratory of Networked Control Systems, Shenyang Institute of Automation, Chinese Academy of Sciences, Shenyang, 110016, China and with Institutes for Robotics and Intelligent Manufacturing, Chinese Academy of Sciences, Shenyang 110016, China and with University of Chinese Academy of Sciences, Beijing, 100049, China. email: {anhaibo, weiliang}@sia.cn

3. Xiaojian Ding and Chunyang Ji are with the Fifth Electronic Institute of MIIT, Guangzhou 510610, China. email: dingxiaojian0923@126.com & 13922248909@139.com.

4. Jindong Tan is with the Department of Mechanical, Aerospace and Biomedical Engineering, University of Tennessee, Konxville, TN, 37996, USA. email: tan@utk.edu

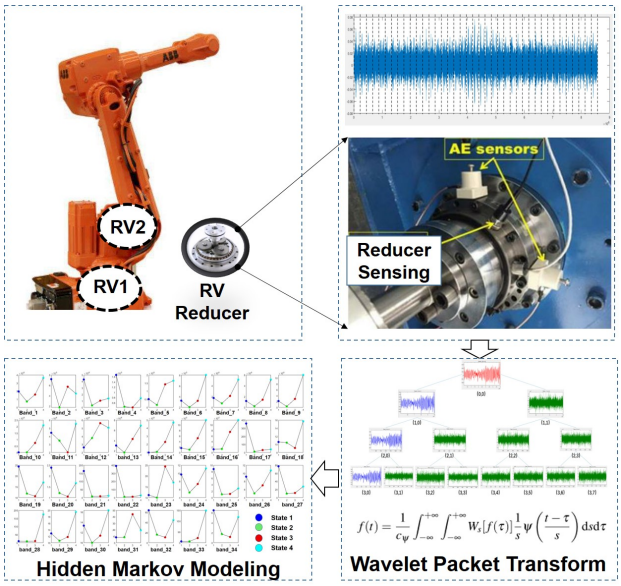


Fig. 1. Framework of the proposed HMM based RV reducer fault detection

A rotate vector (RV) reducer is a typical gear reducer. It is taken as the core component of high-end industrial robots. Compared to other gear reducers, it has higher precision, better reliability, smaller size and impressive efficiency. Usually, RV reducer consists of a two-stage cycloidal design that can provide large torque, high ratio and shock-load capabilities. It utilizes rolling elements to reduce wear and lower backslash with pins and gears from the cycloidal part which provides higher shock resistance. Because of its complex meshing charactersitics and cascade structure, it is rather challenging and time-consuming to detect and localize its damaged components.

Basically, there are three types of RV reducer fault detection methods, i.e., vibration analysis [7]–[9], ferrography analysis [10]–[12] and acoustic emission analysis [13]–[16]. Among these methods, vibration analysis detects the faults by using the spectrum and correlations of vibration signals collected from the vibration sensors attached rigidly to the reducer surface. However, it is not possible to detect the fault occurrence at an early stage (or more specifically, it is unable to detect the faults before the damage has already affected the machine vibrations). As a result, it is quite challenging for the classical vibration analysis to timely detect the occurrence of reducer common faults such as the cracks and their propagations in rotating shafts and pin wheels [15].

978-1-7281-6321-5/19//$31.00 ©2019 IEEE

For the ferrography analysis, the wear particles could be mixed in the liquid lubricants. The analysis on lubricant oil components could be adopted to detect the obvious faults. But this method is time-consuming and only able to detect the faults that have evolved severely in the inner structure [11]. Unlike the vibration monitors that capture the physical behaviours, or the ferrography analyzer that extracts the inner oil lubricant components, acoustic emission (AE) analysis is able to detect the faults by extracting the AE signals propagated within the reducer inner parts. The AE techniques are more likely to extract the hidden fault potential features and predict the fault propagation tendency due to its wider spectrum (the largest frequency could reach up to 1000 KHz [17]), and richer information (the volume of data collected by AE acquisition unit could be 32 MegaBite/sec [18]). By means of AE techniques, the faults could be detected more flexibly, conveniently and earlier. Therefore, this paper seeks to take advantage of AE measurement to detect the RV reducer faults.

Typically, the statistical approaches could be utilized in the AE signal analysis. The models, such as Gaussian Mixture Model (GMM) [19], Decision Tree (DT) [20], Support Vector Machine (SVM) [21] are able to classify the representative features (such as kurtosis [22], entropy [23], energy [24], shape factor [25], crest factor [26]) extracted in both time domain and frequency domain. Among these statistical models, hidden markov model (HMM) is able to correlate the observations and hidden faults in a unified time-series mathematical framework through the observation matrix and state transition matrix. Besides, the fault propagation process satisfies the markov chain that the current state is only related to the previous state and reflected by the observations. Because of these statistical merits, HMM is applied to RV reducer fault detection in this work.

However, there are several issues for the conventional HMM to be applied to reducer fault detections. Usually, the model assumes that the observations (the collected AE signals) have been filtered to suppress the noises before further analysis. But the current observation may not be applied to the observation matrix derivation or hidden state estimation if the sudden disturbance occurs. Besides, there is no systematic way in discretizing the observed signals, which renders the faults characterization challenging.

In order to overcome the above mentioned issues in HMM based RV reducer fault detection, this paper seeks to modify the HMM model in both preprocessing stage and state estimation stage. In the first stage, the wavelet packet transform is utilized to denoise the AE signals in both time and frequency domain. Then HMM is applied to identify the AE parts within each cycle that has 39 subcycles. Through this way, the 39 subcycles could be correctly separated and the curve within each cycle could be further identified. In the second stage, the posteriori probability is modified by taking not only the current observations and the previous state, but also the upcoming observation series. Through this way, the sudden disturbance of AE signals could be suppressed considerably. The contributions of this paper are summarized as follows:

(i) A novel HMM framework is designed that takes not only the current observation and the previous state, but also the upcoming observation series to suppress the sudden acoustic disturbance;

(ii) The wavelet packet transform is adopted to remove the AE noises in both time and frequency domain;

(iii) The HMM is also applied to separate the AE signals within one cycle that has a certain number of subcycles, where the corresponding subcycle features are extracted and used in the corresponding observation matrix.

## II. Methodology

The framework of the proposed approach is shown in Fig. 1. In the first step, the wavelet packet transform is implemented on the raw AE data for denoising. In the second step, the AE signals within each cycle that has 39 subcycles are separated using the HMM; In the second step, the reducer states are classified into four categories: normal state, fault state 1, fault state 2 and fault state 3. The details are described below in the following subsections.

### A. Wavelet Packet Transform for AE Singal Denoising

The AE signal preprocessing (or say denoising) is a critical step for the subsequent procedures in that the collected AE signals are usually accompanied with unexpected mechanical vibration and background noises. Furthermore, the noise will evolve over time that causes problems to denoising using the traditional methods like Fourier Transform. To overcome these issues, the Wavelet Packet Transform (WPT) is adopted that is able to analyze the useful information in both time and frequency domains, with tunable scales and resolutions. WPT is given by

$$f(t) = \frac{1}{c_\psi} \int_{-\infty}^{+\infty} \int_{-\infty}^{+\infty} W_s[f(\tau)] \frac{1}{s} \psi \left( \frac{t-\tau}{s} \right) \mathrm{d}s\mathrm{d}\tau \quad (1)$$

where $s$ represents the wavelet frequency; $t$ denotes the time shift; $c_\psi$ is a constant which is determined by the base function.

$W_s[f(t)]$ is the mother wavelet defined by

$$W_s[f(\tau)] = \int_{-\infty}^{+\infty} f(t) \frac{1}{s} \psi \left( \frac{t-\tau}{s} \right) \mathrm{d}t \quad (2)$$

where $\tau$ and $s$ represent the location and frequency respectively. $W_s$ denotes the amplitude at the specific location.

Through this way, WPT decomposes the signal into various packets $\{P_{j,i}(t)\}$ ($i$ is the packet number and $j$ is the number of levels). For the first level of resolution, the AE signal is composed into two packets $P_{1,0}(t)$ and $P_{1,1}(t)$. $P_{1,0}(t)$ is the lower frequency component; while $P_{1,1}(t)$ is the higher frequency counterpart. For the second level (i.e., $j$=2), each packet is further decomposed into packets $P_{2,0}(t)$, $P_{2,1}(t)$, $P_{2,2}(t)$, $P_{2,3}(t)$; again then these packets are decomposed into $P_{3,0}(t)$, $P_{3,1}(t)$, $P_{3,2}(t)$, $P_{3,3}(t)$, $P_{3,4}(t)$, $P_{3,5}(t)$, $P_{3,6}(t)$, $P_{3,7}(t)$. By means of this process, the AE signals are decomposed into a variety of packets with different time windows and resolutions.

In this paper, the mean energy of WPT coefficients are compared with the pre-set energy threshold $\tau_{en}$. If below $\tau_{en}$, the corresponding packets will be taken as noise. Otherwise, the packets will be considered as the feature packets and preserved for the subsequent classifications.

### B. HMM Based AE Signal Subcycle Separation

For the RV reducer, there exists the difference between the number of cam disk wheel pins and the number of gear pins. When the output shaft and cam disk rotate one circle, the crankshaft will rotate forty circles. Consequently, the period of reunion between the toothed disk and the fixed point of the shell is 39, which also means each rotation cycle of reducer has 39 subcycles.

TABLE I
KURTOSIS AND ENERGY FOR EACH SUBCYLE OF AE SIGNALS.

| **Index** | **1** | **2** | **3** | **4** | **5** | **6** | **7** | **8** |
|---|---|---|---|---|---|---|---|---|
| **Kurtosis** | 4.20 | 3.60 | 3.71 | 3.23 | 3.11 | 3.24 | 3.06 | 3.24 |
| **Energy** | 2.77 | 3.00 | 2.95 | 3.20 | 3.04 | 2.73 | 2.73 | 3.00 |
| **Index** | **9** | **10** | **11** | **12** | **13** | **14** | **15** | **16** |
| **Kurtosis** | 3.1 | 3.23 | 3.82 | 3.81 | 3.36 | 2.89 | 3.20 | 3.39 |
| **Energy** | 3.19 | 3.14 | 3.16 | 3.11 | 2.89 | 2.80 | 2.53 | 2.21 |
| **Index** | **17** | **18** | **19** | **20** | **21** | **22** | **23** | **24** |
| **Kurtosis** | 3.13 | 3.32 | 4.27 | 5.34 | 5.61 | 4.83 | 3.83 | 3.72 |
| **Energy** | 2.55 | 2.57 | 2.72 | 2.98 | 2.94 | 3.13 | 2.98 | 2.95 |
| **Index** | **25** | **26** | **27** | **28** | **29** | **30** | **31** | **32** |
| **Kurtosis** | 3.36 | 3.44 | 3.42 | 2.86 | 3.02 | 3.19 | 3.33 | 2.78 |
| **Energy** | 3.28 | 3.24 | 2.93 | 3.06 | 3.31 | 3.65 | 3.69 | 3.33 |
| **Index** | **33** | **34** | **35** | **36** | **37** | **38** | **39** | |
| **Kurtosis** | 2.89 | 3.28 | 3.14 | 3.66 | 3.22 | 3.18 | 3.66 | |
| **Energy** | 3.15 | 2.72 | 2.73 | 2.57 | 2.45 | 2.47 | 2.67 | |

In order to separate the periods of cycles from the whole AE data, the HMM is applied. Both kurtosis and energy are selected as the feature parameters to perform the separations. For each cycle, there are 39 states, i.e., $\{s_1, s_2, \cdots, s_{39}\}$. The observations for each subcycles of AE signals are evaluated with both kurtosis threshold $\tau_k$ and energy threshold $\tau_e$. By means of this, the observations could be discretized into four types $\{o_1, o_2, o_3, o_4\}$. For instance, in the subcycle $i$, the relationship between the discretized observation and the corresponding kurtosis $k_i$, energy $e_i$ could be expressed as

$$\begin{array}{ll} observation = o_1 & k_i \le \tau_k, e_i \le \tau_e \\ observation = o_2 & k_i \le \tau_k, e_i > \tau_e \\ observation = o_3 & k_i > \tau_k, e_i \le \tau_e \\ observation = o_4 & k_i > \tau_k, e_i > \tau_e \end{array} \tag{3}$$

In this case, there will be $n$ states for subcycles ($n$=39) and $m$ observations ($m$=4). The transition matrix $A_{ss}$ and the observation matrix $B_{ss}$ are given by

$$A_{ss} = \begin{bmatrix} a_{11} & a_{12} & .. & .. & a_{1n} \\ a_{21} & a_{22} & .. & .. & a_{2n} \\ . & . & . & . & . \\ . & . & . & . & . \\ a_{n1} & a_{n2} & .. & .. & a_{nn} \end{bmatrix} \tag{4}$$

$$B_{ss} = \begin{bmatrix} b_{11} & b_{12} & .. & b_{1m} \\ b_{21} & b_{22} & .. & b_{2m} \\ . & . & . & . \\ . & . & . & . \\ b_{n1} & b_{n2} & .. & b_{nm} \end{bmatrix} \tag{5}$$

### C. HMM Based RV Reducer Fault Classification

As a special model among dynamic Bayesian networks, HMM is able to derive the hidden state sequence from the observation sequence. Since the hidden state is unobservable, it can only be implied from the corresponding observation and the previous state.

HMM is typically designed to solve three fundamental problems: modeling, evaluation and decoding. In this section, modeling for the HMM in our case will be firstly introduced. Then the corresponding evaluation and decoding will be presented.

HMM consists of transition matrix $A$, observation matrix $B$ and initial state vector $\pi$. The triplet $\lambda = \{\pi, A, B\}$ is modelled that is able to maximize the probability $P(o|\lambda)$. In this paper, the observation sequence $\{o_1, o_2, \cdots, o_n\}$ which could be calculated by the kurtosis sequence $\{kur_1, kur_2, \cdots, kur_n\}$ and the energy sequence $\{e_1, e_2, \cdots, e_n\}$, i.e., $o_{i,1\le i\le n} = kur_i\left(\tau_2 \cdot kur_i{}^2 + \tau_1 \cdot kur_i + \tau_0\right)$. The Baum-Welch method [27] is applied to estimate the triplet $\lambda$. It iterates between two steps: the expectation step and maximization step. From the existing model $\lambda_0$, which is randomly selected or roughly approached by experiences), the objective function $P(o|\lambda)$ will be transformed into a new function $\varphi(\lambda_1, \lambda_0)$ that measures the divergence between the previous model $\lambda_0$ and the updated model $\lambda_1$.

In this paper, there are four reducer health conditions, i.e., $S1$: $Health$; $S2$: $Fault1$ (least severe); $S3$: $Fault2$ (medium severe); $S4$: $Fault3$ (most severe). These four states observe the left-right transition model. The RV reducer will be at health condition initially. After a certain period of operations, there will be some gentle faults, such as the abrasions on the crank shaft contact surface; then the fault will evolve from the medium level to the most severe level over time. Unlike the ergodic type, that each state could transit to any other state, the reducer fault state can only evolve from the left to right (from the healthy to the damaged).

In case of the RV reducer fault detection, the observed AE signals are usually accompanied with unexpected and unknown disturbance. For instance, at time instant $i$, the hidden state $s_i$ deduced from the outlier $o_i$ would be mistaken. What is worse, the next state $s_{i+1}$ will rely on the current state, which would result in the erroneous hidden state sequence. In order to overcome this issue, different from the conventional HMM our model considers not only the current observation $o_i$, but also the upcoming number of observations $\{o_{i+1}, \cdots, o_{i+m}\}$.Since the disturbance could only last for a short periods of time, the disturbance impacts could be considerably suppressed through the joint posteriori probability $P(s_{i+1}|s_i, \{o_{i+1}, \cdots, o_{i+m+1}\}, \lambda)$. Through this way, the state $s_i$ could be selected by the majority voting as

follows:

$$s_i = \text{argmax}_{s_i}\left(N(s_1), N(s_2), N(s_3), N(s_4)\right) \tag{6}$$

where $N(s_1), N(s_2), N(s_3), N(s_4)$ are determined by the sum of corresponding states which are calculated by the Viterbi method.

## III. Experiments and Analysis

### A. Experimental Setup

In order to verify the performance of the proposed RV reducer fault detection performance, we have developed the reducer experimental platform, as shown in Fig. 2. It mainly consists of five components, namely, drive motor, torque sensor, RV reducer, magnetic power brake and AE signal acquisition equipment. The drive motor offers the rotation energies. Its speed ranges between $0 \sim 2000$ r/min. The range of input torque sensor is 50 N·m with measurement error less than 0.5%. The magnetic power provides the load that could reach up to 5000 N·m. In this work, the RV reducer is the typical 40-$E$ series from the Nabtesco company in Japan[1]. The reduction ratio for this RV is 121.

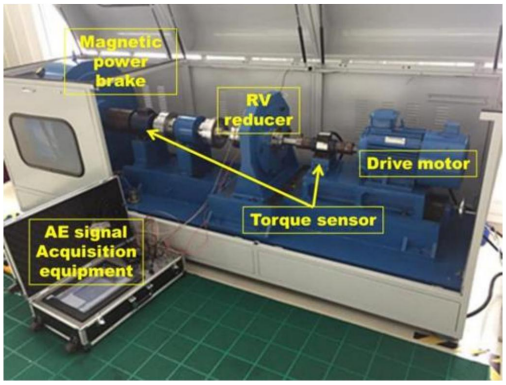


Fig. 2. RV reducer experimental platform.

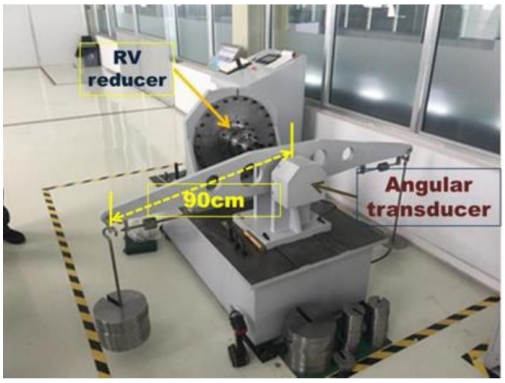


Fig. 3. Return difference equipment

To evaluate the RV reducer damage level, the return difference equipment is developed, as shown in Fig. 3. In the evaluation process, the RV is fixed on the pedestal, the corresponding torque is measured by placing the equivalent standard metal weights on plate. Through this way, the angular value could be observed by the angular transducer.

In the test rig, two AE sensors are rigidly attached to the surface of reducer output outer ring, shown in Fig. 4. By means of this configuration, the sensors could sample the AE data more precisely, since the signal attenuation from the signal source to the sampling articles are considerably alleviated. In our setup, the two AE sensors are placed in a parallel manner and the sampled data are synchronized by timestamps. Apart from that, the vibration and temperature sensors are also placed on the surface of RV, the corresponding vibration measurements and instrument temperature values are collected in the acquisition equipment.

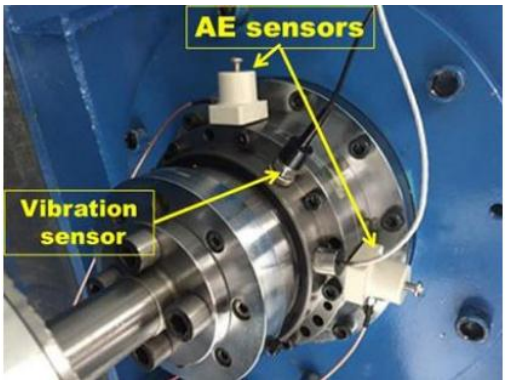


Fig. 4. Configuration of AE sensors

### B. Tests and Analysis

Totally, there are 252 groups of tests conducted in the experiment. The reducer rotation speeds are selected with 7 values, namely, 4 r/min, 6 r/min, 8 r/min, 10 r/min, 12 r/min, 14 r/min and 16 r/min. Besides, we set seven rotation speeds for output shaft, namely, 150 N·m, 200 N·m, 250 N·m, 300 N·m, 350 N·m and 400 N·m. After combining these workloads with rotation speeds, we set the rotation load torque to 1000 N·m with output rotation speed to 15 r/min and kept the RV running for two hours straight and continuously to simulate the overload test. Then the return difference is measured to evaluate the RV damage level.

In the overload test, the Arrhenius model [28] is applied. The wear tendency could be inferred by measuring the return differences. The return difference are calculated after each overload test for five times, as shown in Table II. It can be seen that the return difference becomes larger after each load test. The return difference will increase each time for 10" (unit is in angular second). In our case, the "health" state is reflected by the return difference less than 12"; "least severe" state is reflected by the return difference between 12" and 21"; "medium severe" state is reflected by the return difference between 21" and 32"; "most severe" state is reflected by the return difference between 32" and 46".

After WPT using *db*5 mother wavelet, the discriminant frequency bands were selected. In our case, we manually choose 34 frequency bands that preserve relatively apparent

[1]https://www.nabtescomotioncontrol.com/pdfs/RVseries.pdf

TABLE II

RETURN DIFFERENCE AFTER OVERLOAD TEST

| Test No. | 1 | 2 | 3 | 4 |
|---|---|---|---|---|
| Forward (angular second) | 7” | 19” | 22” | 33” |
| Backward (angular second) | -5” | -2” | -10” | -13” |
| Return difference (angular second) | 12” | 21” | 32” | 46” |

energy features. These frequency bands are listed in Table III. The frequency interval is selected approximately 50Hz that covers the main components inside.

For each state, the AE signals have been collected 12 times. The energies for each cycle are calculated using the norm-2 operations. Totally, there will be $12*34=408$ groups of AE signals. The energy distribution on the 34 frequency bands for these four states is shown in Fig. 5. The symbols “*”, “solid circle”, “star” and “plus” represent $State1$, $State2$, $State3$ and $State4$ respectively. It can be seen that some energies have similar distributions, which poses considerable challenges in discriminating the corresponding state labels.

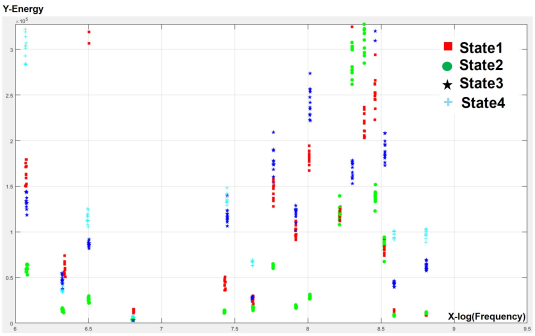


Fig. 5. The energies among the $34th$ frequency bands

## IV. CONCLUSION

In this paper, a novel RV reducer fault detection method is proposed using the acoustic emission (AE) measurements. Firstly, the wavelet packet transform (WPT) is implemented to denoise the AE signals. Secondly, HMM is applied to separate the AE signal bulks within one cycle that has 39 subcycles. Eventually, HMM model is modified that takes not only the current observations and previous states, but also the subsequent series of observations within the posteriori probability framework, to infer the RV state sequence. Through this way, the random and unknown disturbance could be considerably suppressed. The proposed method has been evaluated on our developed RV platform. The analysis on recognition rate and return difference could prove the effectiveness of the fault detection model.

## ACKNOWLEDGMENT

The authors would like to thank the editor and reviewers for their valuable suggestions and comments.

This work has been supported in part by the National Key Research and Development Program of China (2017YFE0101200 and 2017YFE0123000), the Key Research and Development Program of Guangdong Province (2019B090916001), National Natural Science Foundation of China (71661147005 and 61903357), International Partnership Program of Chinese Academy of Sciences (173321KYSB20180020), Liaoning Provincial Natural Science Foundation of China (2019-YQ-09), and Pearl River Nova Program of Guangzhou (201605131121390).

## REFERENCES

[1] R. V. Petrescu, R. Aversa, A. Apicella, M. Mirsayar, S. Kozaitis, T. Abu-Lebdeh, and F. I. Petrescu, “Analysis and synthesis of mechanisms with bars and gears used in robots and manipulators,” *Journal of Mechatronics and Robotics*, vol. 1, no. 2, pp. 98–108, 2017.

[2] G. Fagogenis, V. De Carolis, and D. M. Lane, “Online fault detection and model adaptation for underwater vehicles in the case of thruster failures,” in *2016 IEEE International Conference on Robotics and Automation (ICRA)*. IEEE, 2016, pp. 2625–2630.

[3] Y. Trachi, E. Elbouchikhi, V. Choqueuse, and M. E. H. Benbouzid, “Induction machines fault detection based on subspace spectral estimation,” *IEEE Transactions on Industrial Electronics*, vol. 63, no. 9, pp. 5641–5651, 2016.

[4] P. Wang, J. Li, and Y.-Q. Jin, “A study on the design of slicing cutter for cycloid gear based on conjugate theory,” *The International Journal of Advanced Manufacturing Technology*, vol. 98, no. 5-8, pp. 2057–2068, 2018.

[5] J. Al Hage, M. E. El Najjar, and D. Pomorski, “Multi-sensor fusion approach with fault detection and exclusion based on the kullback–leibler divergence: Application on collaborative multi-robot system,” *Information Fusion*, vol. 37, pp. 61–76, 2017.

[6] Z. Gao, C. Cecati, and S. X. Ding, “A survey of fault diagnosis and fault-tolerant techniquesłpart i: Fault diagnosis with model-based and signal-based approaches,” *IEEE Transactions on Industrial Electronics*, vol. 62, no. 6, pp. 3757–3767, 2015.

[7] M. Farina, E. Osto, A. Perizzato, L. Piroddi, and R. Scattolini, “Fault detection and isolation of bearings in a drive reducer of a hot steel rolling mill,” *Control Engineering Practice*, vol. 39, pp. 35–44, 2015.

[8] P. Peng and J. Wang, “Noscnn: A robust method for fault diagnosis of rv reducer,” *Measurement*, 2019.

[9] R. Duan and F. Wang, “Fault diagnosis of on-load tap-changer in converter transformer based on time–frequency vibration analysis,” *IEEE Transactions on Industrial Electronics*, vol. 63, no. 6, pp. 3815–3823, 2016.

[10] P. Peng and J. Wang, “Wear particle classification considering particle overlapping,” *Wear*, 2019.

[11] S. Wang, T. Wu, H. Wu, and N. Kwok, “Modeling wear state evolution using real-time wear debris features,” *Tribology & Lubrication Technology*, vol. 74, no. 11, pp. 86–100, 2018.

[12] Z. Duan, T. Wu, S. Guo, T. Shao, R. Malekian, and Z. Li, “Development and trend of condition monitoring and fault diagnosis of multi-sensors information fusion for rolling bearings: a review,” *The International Journal of Advanced Manufacturing Technology*, vol. 96, no. 1-4, pp. 803–819, 2018.

[13] W. Caesarendra, B. Kosasih, A. K. Tieu, H. Zhu, C. A. Moodie, and Q. Zhu, “Acoustic emission-based condition monitoring methods: Review and application for low speed slew bearing,” *Mechanical Systems and Signal Processing*, vol. 72, pp. 134–159, 2016.

[14] C. Gómez Muñoz and F. García Márquez, “A new fault location approach for acoustic emission techniques in wind turbines,” *Energies*, vol. 9, no. 1, p. 40, 2016.

[15] F. Hemmati, W. Orfali, and M. S. Gadala, “Roller bearing acoustic signature extraction by wavelet packet transform, applications in fault detection and size estimation,” *Applied Acoustics*, vol. 104, pp. 101–118, 2016.

[16] M. Elforjani and S. Shanbr, “Prognosis of bearing acoustic emission signals using supervised machine learning,” *IEEE Transactions on Industrial Electronics*, vol. 65, no. 7, pp. 5864–5871, 2017.

[17] A. V. Filippov, V. Rubtsov, and S. Y. Tarasov, “Acoustic emission study of surface deterioration in tribocontacting,” *Applied Acoustics*, vol. 117, pp. 106–112, 2017.

[18] H. An, W. Liang, Y. Zhang, Y. Li, Y. Liang, and J. Tan, “Rotate vector reducer crankshaft fault diagnosis using acoustic emission techniques,” in *2017 5th International Conference on Enterprise Systems (ES)*. IEEE, 2017, pp. 294–298.

TABLE III

THE SELECTED FREQUENCY BANDS FROM WPT

| **Index** | Band 1 | Band 2 | Band 3 | Band 4 | Band 5 | Band 6 |
|---|---|---|---|---|---|---|
| **Frequency (Hz)** | [410,450] | [530,570] | [640,680] | [870,910] | [1640,1710] | [2020,2060] |
| **Index** | Band 7 | Band 8 | Band 9 | Band 10 | Band 11 | Band 12 |
| **Frequency (Hz)** | [2330,2370] | [2680,2800] | [2950,3050] | [3670,3740] | [4000,4050] | [4350,4420] |
| **Index** | Band 13 | Band 14 | Band 15 | Band 16 | Band 17 | Band 18 |
| **Frequency (Hz)** | [4680,4800] | [4990,5050] | [5350,5380] | [6660,6710] | [149500,150000] | [198200,198400] |
| **Index** | Band 19 | Band 20 | Band 21 | Band 22 | Band 23 | Band 24 |
| **Frequency (Hz)** | [224500,225000] | [275000,275400] | [299800,299900] | [325500,326000] | [348100,348500] | [374700,375300] |
| **Index** | Band 25 | Band 26 | Band 27 | Band 28 | Band 29 | Band 30 |
| **Frequency (Hz)** | [362200,362400] | [374700,375200] | [387600,387800] | [397050,397350] | [398600,399000] | [401400,401800] |
| **Index** | Band 31 | Band 32 | Band 33 | Band 34 | | |
| **Frequency (Hz)** | [426800,427000] | [449300,449600] | [473800,474000] | [550400,550800] | | |


[19] L. Cai, X. Tian, and S. Chen, "Monitoring nonlinear and non-gaussian processes using gaussian mixture model-based weighted kernel independent component analysis," *IEEE transactions on neural networks and learning systems*, vol. 28, no. 1, pp. 122–135, 2017.

[20] R. Yan, Z. Ma, Y. Zhao, and G. Kokogiannakis, "A decision tree based data-driven diagnostic strategy for air handling units," *Energy and Buildings*, vol. 133, pp. 37–45, 2016.

[21] Z. Yi and A. H. Etemadi, "Line-to-line fault detection for photovoltaic arrays based on multiresolution signal decomposition and two-stage support vector machine," *IEEE Transactions on Industrial Electronics*, vol. 64, no. 11, pp. 8546–8556, 2017.

[22] A. Steinwolf, "Vibration testing of vehicle components by random excitations with increased kurtosis," *International Journal of Vehicle Noise and Vibration*, vol. 11, no. 1, pp. 39–66, 2015.

[23] G. L. McDonald and Q. Zhao, "Multipoint optimal minimum entropy deconvolution and convolution fix: Application to vibration fault detection," *Mechanical Systems and Signal Processing*, vol. 82, pp. 461–477, 2017.

[24] Y. Imaouchen, M. Kedadouche, R. Alkama, and M. Thomas, "A frequency-weighted energy operator and complementary ensemble empirical mode decomposition for bearing fault detection," *Mechanical Systems and Signal Processing*, vol. 82, pp. 103–116, 2017.

[25] J. B. Ali, N. Fnaiech, L. Saidi, B. Chebel-Morello, and F. Fnaiech, "Application of empirical mode decomposition and artificial neural network for automatic bearing fault diagnosis based on vibration signals," *Applied Acoustics*, vol. 89, pp. 16–27, 2015.

[26] O. Janssens, V. Slavkovikj, B. Vervisch, K. Stockman, M. Loccufier, S. Verstockt, R. Van de Walle, and S. Van Hoecke, "Convolutional neural network based fault detection for rotating machinery," *Journal of Sound and Vibration*, vol. 377, pp. 331–345, 2016.

[27] J. Zhang, F. Wang, Z. Zhong, and S. Wang, "Continuous phase modulation classification via baum-welch algorithm," *IEEE Communications Letters*, vol. 22, no. 7, pp. 1390–1393, 2018.

[28] S. H. Shahcheraghi, G. R. Khayati, and M. Ranjbar, "An advanced reaction model determination methodology in solid-state kinetics based on arrhenius parameters variation," *Journal of Thermal Analysis and Calorimetry*, vol. 126, no. 2, pp. 981–993, 2016.